Electronic Supplementary Material (ESI) for Nanoscale.

Supplementary Information

Defect Engineering As a Versatile Route to Estimate Various Scattering Mechanisms in Monolayer Graphene on Solid Substrates

Pawan Kumar Srivastava and Subhasis Ghosh*

School of Physical Sciences, Jawaharlal Nehru University, New Delhi-110067(India)

*email: subhasis.ghosh.jnu@gmail.com

Contents:

S1.0 Raman G and 2D peak positions of graphene prepared in polar and non polar solvents:

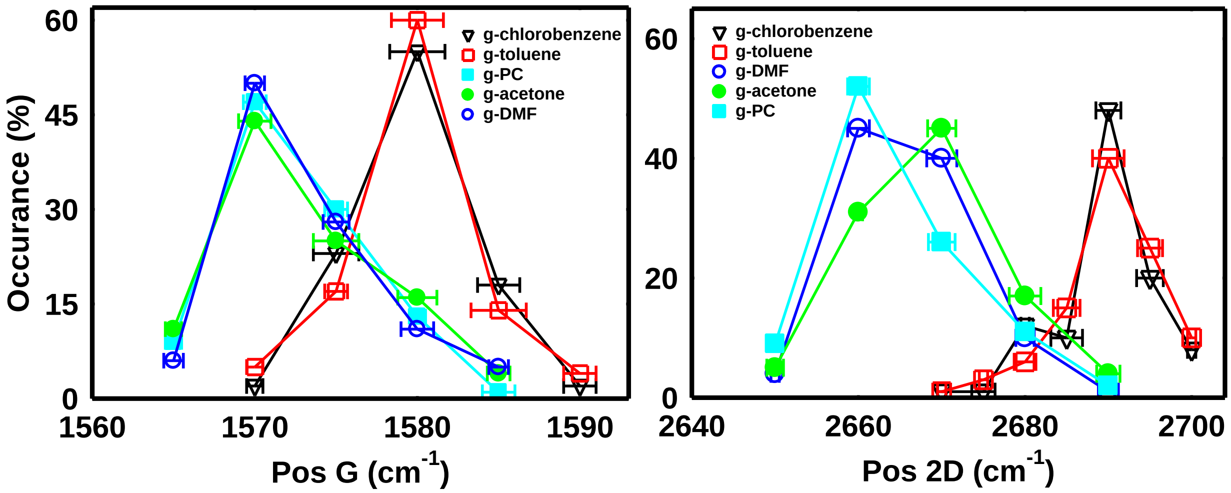

Figure S1: Raman G and 2D peak position of graphene flakes prepared various solvents. It is evident that maxima of G peak falls near 1580 cm^{-1} and 1570 cm^{-1} for graphene prepared in non-polar and polar solvents, respectively. Similarly, maxima for 2D peak falls near 2690 cm^{-1} and (2665 ± 5) cm^{-1} for graphene prepared in non-polar and polar solvents, respectively. Connecting lines are guide for eyes.

S2.0 Effect of sonication on defect induced Raman D band in graphene exfoliated in non-polar and polar environment:

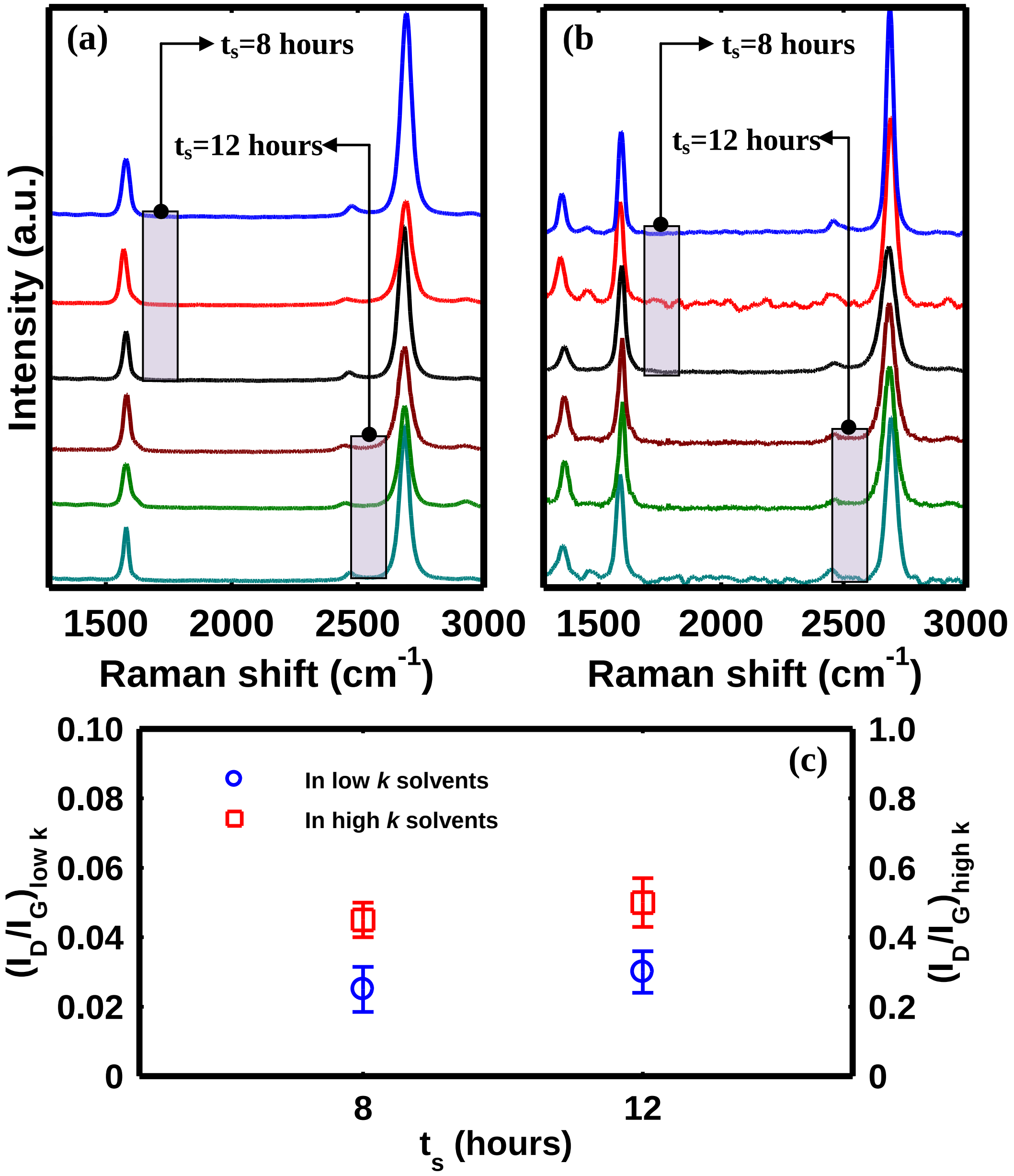

Figure S2: Raman spectra of graphene layers exfoliated in **(a)** low *k* solvents and **(b)** high *k* solvents. Spectra for two different sonication time (t_s = 8 hours and 12 hours) are given as indicated by arrows. Absence of D band in case of graphene exfoliated in low *k* solvents and enhanced D peak in high *k* solvents under identical conditions indicate sonication has negligible impact in defect incorporation. **(c)** Evolution in normalized D band intensity (I_D/I_G) with t_s for graphene layers exfoliated in low and high *k* solvents.

As elucidated in Figure S2, by increasing the sonication time from 8 hours to 12 hours negligible variation in normalized D band intensity (I_D/I_G) was observed for graphene layers exfoliated in both, low and high *k* solvents. Moreover, it is to be noted that to obtain graphene layers, experimental conditions (*i.e.* sonication time, centrifugation time, etc.) were kept identical and only dielectric constant of the solvents was varied and then solvents were removed by vacuum annealing at a temperature typically more than the boiling point of the solvents. If we compare electrical characteristics and Raman spectroscopic results given in Figure 1 (in main paper), variation in position of the Dirac point and evolution of D band in case of graphene exfoliated in high *k* solvents, clearly indicate that sonication does not have dominating role in incorporation of defects in graphene basal plane otherwise, effect of sonication induced defects should have been observed in both, low and high *k* solvents.

We have also observed that increase in sonication time results into cutting of graphene flakes which may cause edge defects. We have performed confocal Raman imaging on graphene samples (t_s=12 hours). Figure S3 shows representative confocal Raman images for graphene layers exfoliated in low and high *k* environments. Raman images generated by the intensity of D band clearly indicate that even after prolonged sonication time only edge defects (minimal) are present in graphene exfoliated in low *k* solvents. Whereas, defect density is more pronounced in graphene samples exfoliated in high k solvents. This suggests that observed Raman D peak is not at all governed by the sonication induced damage of graphene flakes, but covalent attachment of solvent molecules to graphene surface is responsible for evolution of D peak in high *k* environment. Detail discussion on the possibility of molecular attachment and its effect on evolution of the Raman D band in high *k* solvents will be discussed later in this suppl. information.

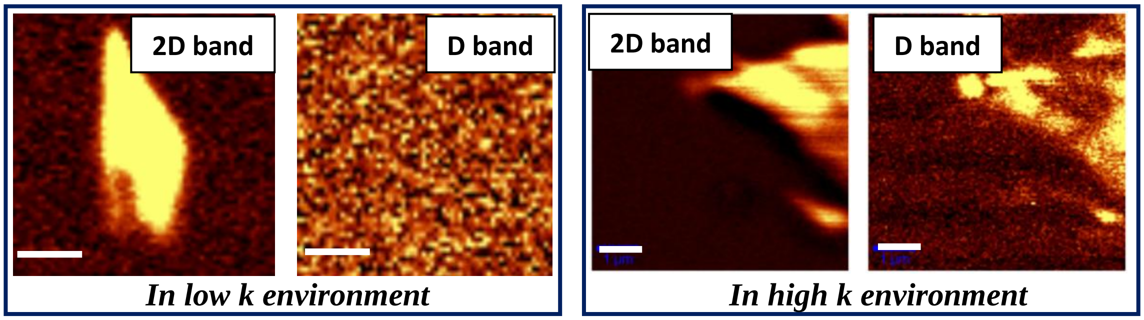

Figure S3: Confocal Raman images generated by the intensity of 2D and D bands for graphene exfoliated in low and high *k* environment. Scale bars: for low *k*-2μm ; for high *k*-1μm.

S3.0 Gate capacitance measurement on graphene devices:

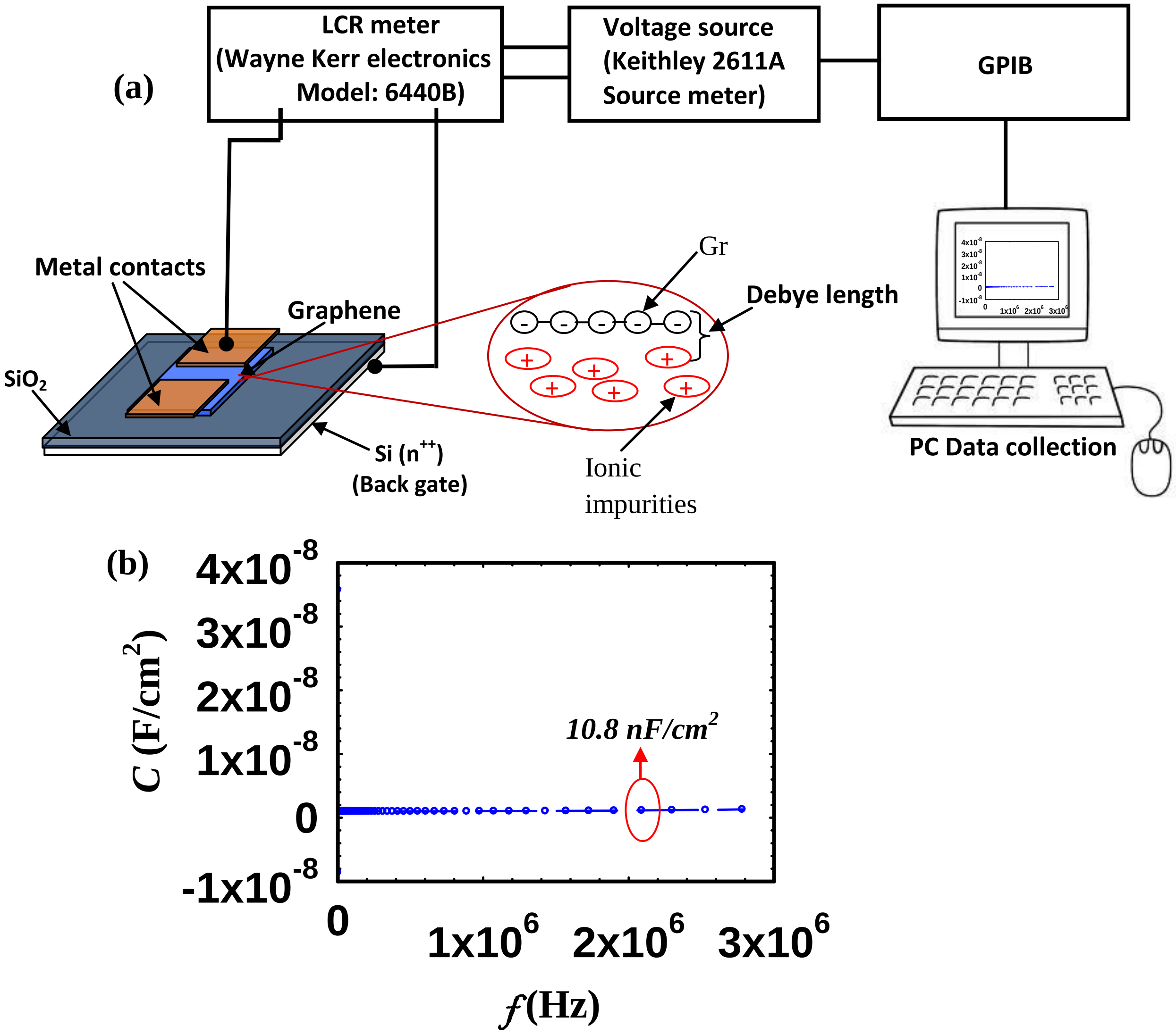

Figure S4: (a) Schematics of Capacitance-frequency (*c*-*f*) measurement on graphene based devices. To acquire *c*-*f* measurement frequency was sweeped from 30Hz to 3MHz at fixed bias of 2.0V. Formation of electrical double layer[1] (EDL) is also schematically shown. In case of polar solvents, Debye length for EDL comes out to be~500 nm, indicating minimal contribution from coulomb scattering due to solvent impurities. Gr signifies the carriers in graphene layers and positive ions indicate impurities in liquids. **(b)** Capacitance v/s frequency curve showing capacitance/area ~ 10.8 nF/cm^2. In graphene monolayer (prepared in non-polar solvents) based devices, the total capacitance could be solely attributed to geometric capacitance (no ions would be present in non-polar solvents) given by $C_g = k.A/d$. In case of graphene monolayers prepared in polar solvents there would also be a contribution of electrical double layer capacitance. Since Debye length in our devices is as large as ~ 500 nm, effect of double layer capacitance can be neglected. Moreover, it can be observed from the capacitance data that capacitance is almost independent of frequency (low and high) which itself signifies the absence of impurity ions near graphene surface.

S3.1 Determination of carrier mobility: Relevance of capacitance measurement:

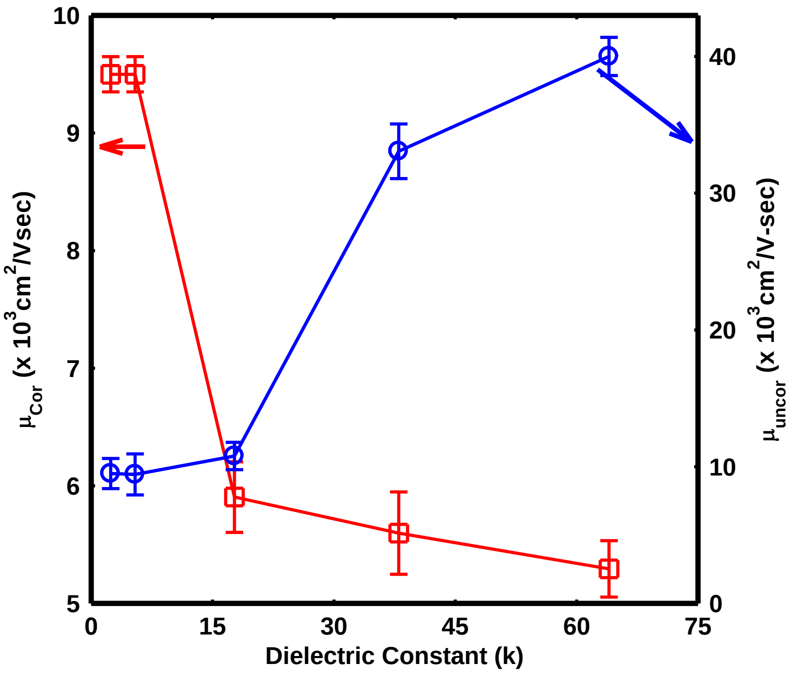

Figure S5: Dependence of carrier mobility on dielectric constant of the solvents used for exfoliation of graphene layers. Carrier mobility μ_{uncor}, calculated considering fixed gate capacitance ~ 11.5 nF/cm^2 corresponding to SiO$_2$ (300 nm) and μ_{cor}, calculated using experimentally measured gate capacitance for each devices. In manuscript, μ_{cor} has been denoted as μ_{cor} for simplicity. Connecting lines are guide for eyes. Error bars denote uncertainty in carrier mobility measured on various graphene based devices. It is clear that when we have taken the calculated capacitance on individual devices into account, almost opposite trend in mobility variation has been observed. Hence, capacitance measurement has a strong role in determining the correct carrier mobility in our devices.

S4.0 Raman spectra and electrical characterization of g-toluene, g-acetone and g-DMF:

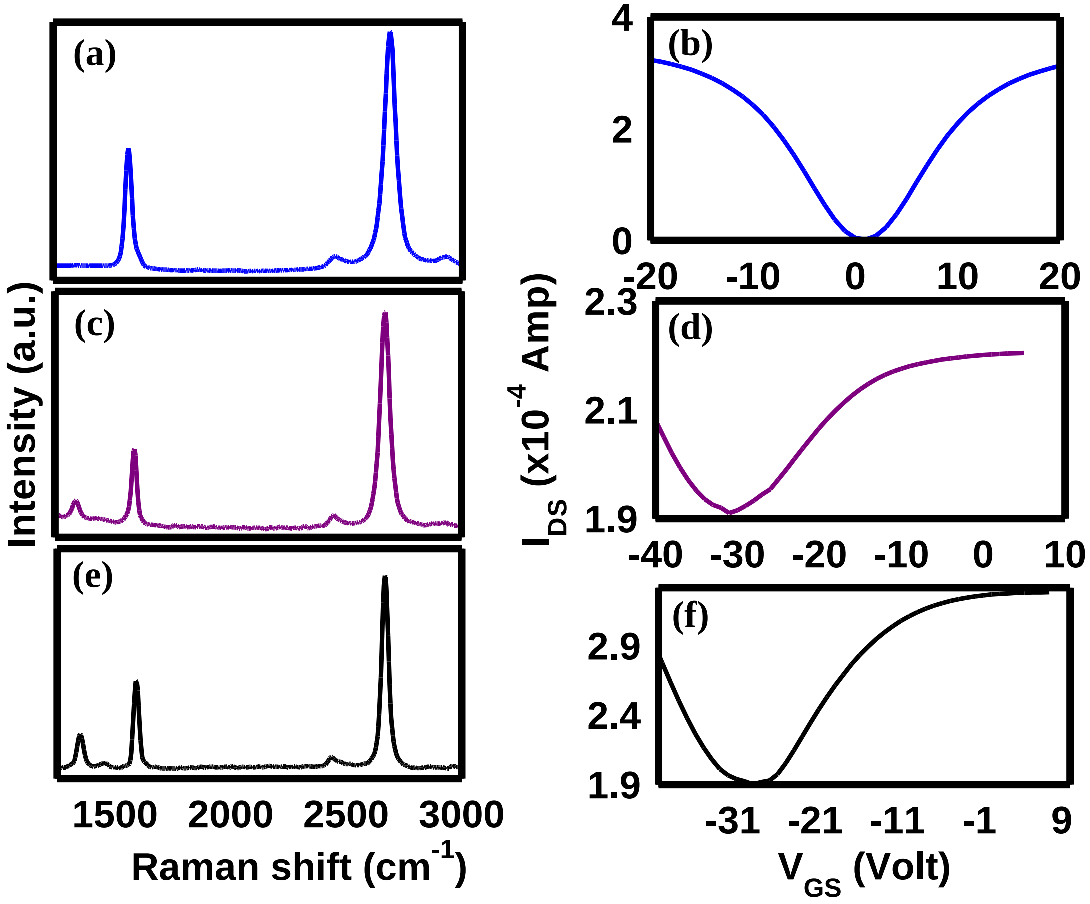

Figure S6: Raman spectra and transfer characteristics of FET based on graphene layers exfoliated in **(a,b)** toluene, **(c,d)** acetone and **(e,f)** DMF. Raman peaks of G and 2D bands are at (1580 cm^{-1}; 2690 cm^{-1}); (1575 cm^{-1}; 2670 cm^{-1}); and (1570 cm^{-1}; 2665 cm^{-1}) for *g*-toluene, *g*-acetone and *g*-DMF, respectively. It is clear that D peak intensity in *g*-toluene is negligible whereas, in case of *g*-acetone and *g*-DMF, D peak intensity is significant. Dirac points are at ~ 1.0V for *g*-toluene and around -30.0V for *g*-acetone and *g*-DMF as indicated by arrows reveals the pristine and doped/disordered behavior of graphene layers[2,3].

S5.0 Schematic of the scanning tunneling microscopy on graphene based devices:

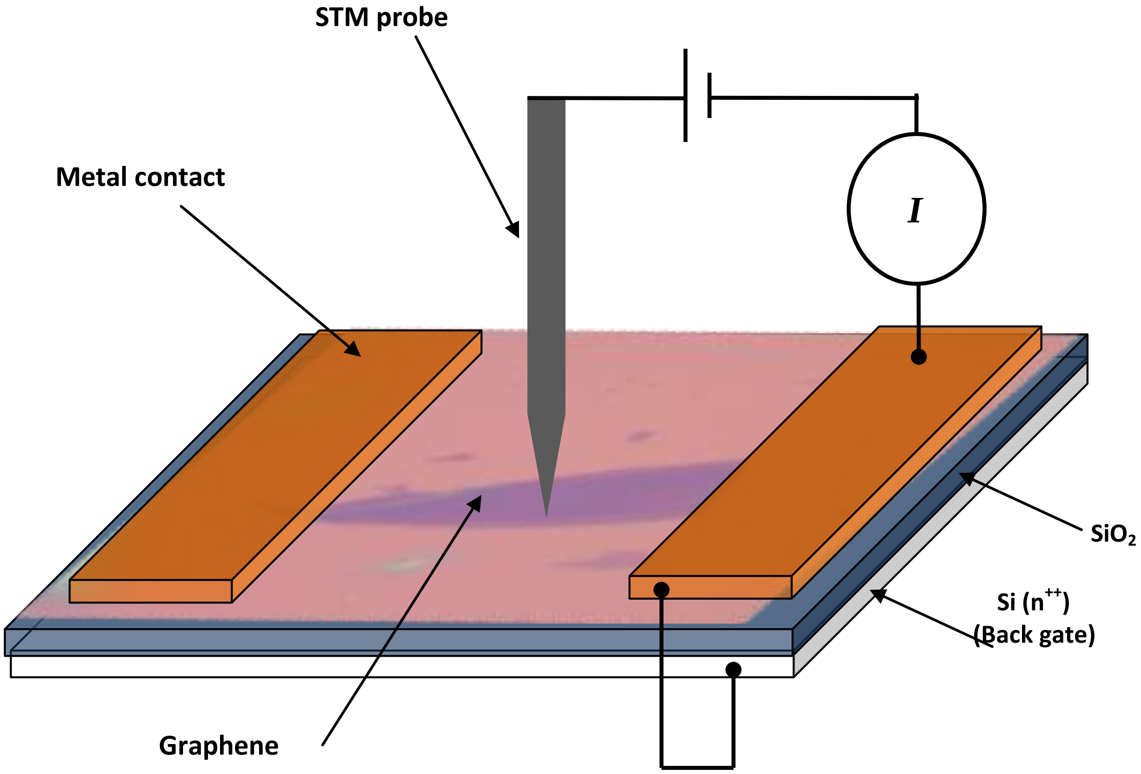

Figure S8. Schematic diagram of the STM measurement on graphene based devices.

S6.0 Raman D peak of graphene layers exfoliated in non-polar solvents:

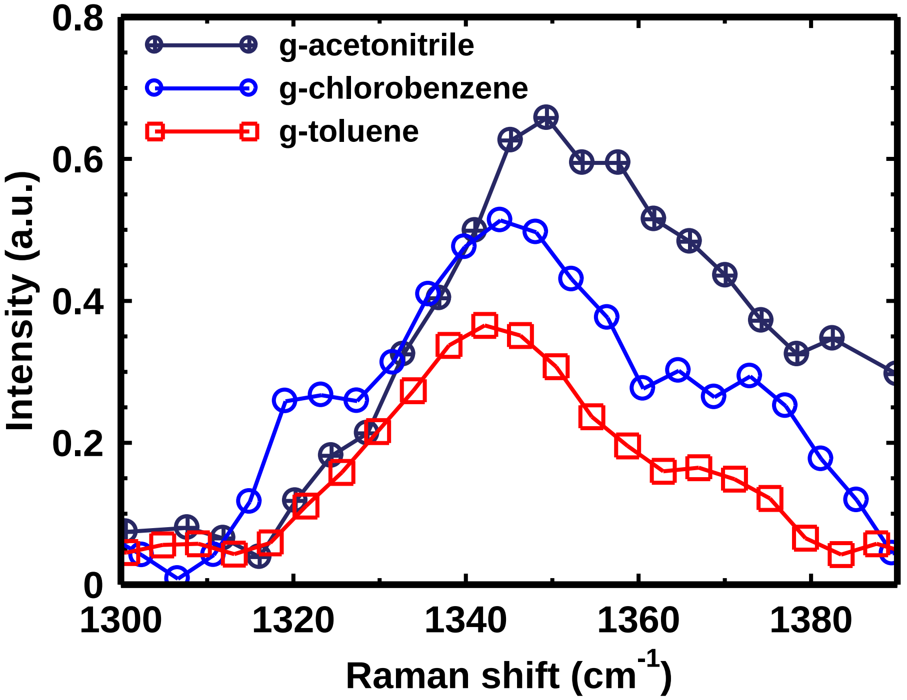

Figure S8. Raman D peaks of graphene layers exfoliated in solvents with low dielectric constant. Spectra are presented after zooming the corresponding region (~ 100 times). Although, *g*-toluene, *g*-chlorobenzene and *g*-acetonitrile (not included in this work) show pristine behavior but diminutive D peak intensities indicate the presence of low concentration of point defects which results L_D ~ 30 nm. Connecting lines are guide for eyes.

S7.0 Infrared spectroscopic measurement:

To substantiate the doping induced defects or more specifically, to understand whether covalent bonding or supramolecular interaction between graphene and solvent molecules is responsible for defects (dopants), we have carried out infrared spectroscopic measurements on graphene samples grown in low and high dielectric solvents. Figure S8 and S9 represent IR spectra of bare solvents (toluene and PC) and graphene grown in respective solvents (*g*-toluene and *g*-PC). IR spectroscopy of graphene on SiO_2 /Si substrate was done using Varian-7000 UMA-600 IR microscope, in reflectance mode by inspecting individual graphene layers under microscope using IR source with excitation wavelength of 1064 nm.

S7.1 Infrared spectra of toluene and g-toluene:

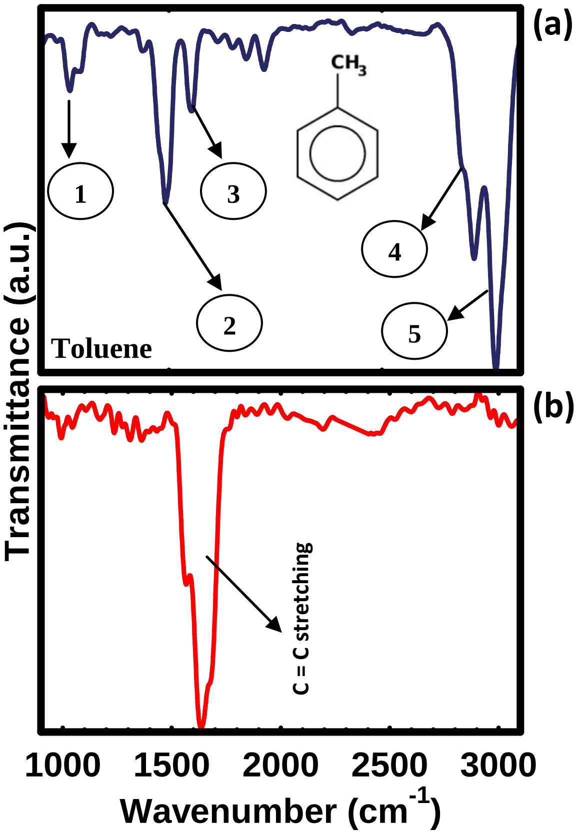

1- C-H bending (alkyl)
2- C-C stretching (aromatic)
3- C-C stretching (aromatic)
4- C-H in plane stretching (alkyl)
5- C-H in plane stretching (aromatic)

Figure S9. Infrared spectra of **(a)** toluene and **(b)** graphene layer obtained by exfoliation of HOPG in toluene (*g*-toluene). Prominent peaks have been labeled with associated vibrations. Molecular structure of toluene is also given in inset

In bare toluene, we can observe five prominent peaks at 1033 cm^{-1}, 1485 cm^{-1}, 1608 cm^{-1}, 2936 cm^{-1} and 3030 cm^{-1}. First peak at 1485 cm^{-1} corresponds to C-H bending of alkyl group attached to aromatic ring, peaks at 1485 cm^{-1}and 1608 cm^{-1} are attributed to in plane aromatic C-C stretching and last two peaks facilitates in plane alkyl and aromatic C-H stretching, respectively[4,5]. In *g*-toluene (Figure S8-b), only C=C stretching at 1635 cm^{-1} can be observed and all other vibrational modes are absent. Minor shifts in C=C vibrations were also observed in IR spectra of *g*-toluene as compared to that of bare toluene. This is attributed to the difference in the aromatic structure of toluene and graphene (no hydrogen in aromatic ring). Indication, we get from IR spectra of *g*-toluene is unambiguous that these graphene layers exhibit pristine behavior and are not functionalized.

S7.2 Infrared spectra of PC and g-PC:

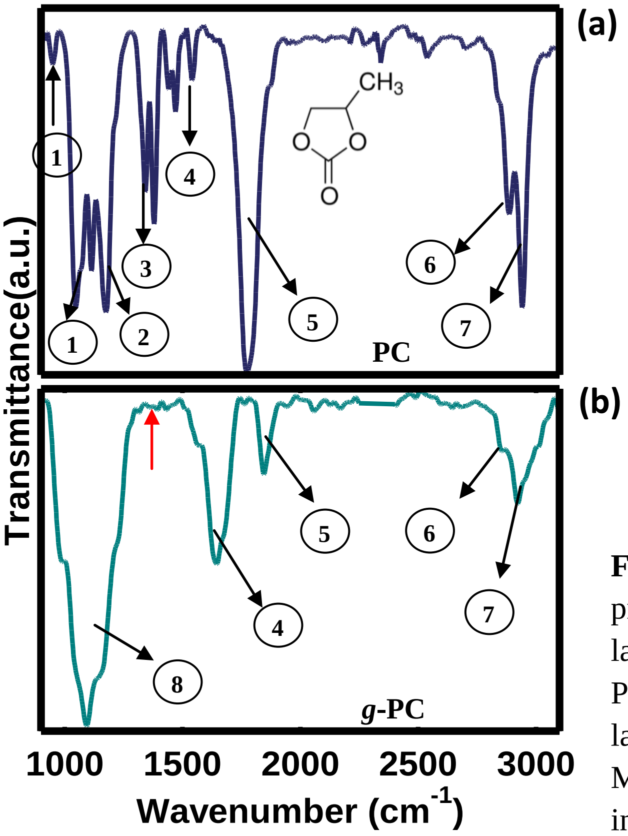

1- C-H bending (alkyl)
2- C-O stretching
3- C-H stretching (rocking/bending)
4- C-C in plane stretching (aromatic)
5- C=O stretching
6- C-H in plane stretching (alkyl)
7- C-H in plane stretching (aromatic)
8- See description below

Figure S10: Infrared spectra of **(a)** propylene carbonate (PC) and **(b)** graphene layer obtained by exfoliation of HOPG in PC (*g*-PC). Prominent peaks have been labeled with associated vibrations. Molecular structure of PC is also given in inset.

In PC, seven prominent peaks[6,7] were observed at 980 cm^{-1} and 1030 cm^{-1} (both for alkyl C-H bending), 1140 cm^{-1} (C-O), 1349 cm^{-1} and 1450 cm^{-1} (both for C-H rocking and bending respectively), 1605 cm^{-1} (C-C, aromatic), 1755 cm^{-1} (C=O), 2931 cm^{-1} and 3035 cm^{-1} attributed to the in plane alkyl and aromatic C-H stretching, respectively. In *g*-PC, five significant peaks were observed (see Figure S9), but if we de-convolute the peak labeled as 8, we get five peaks at 980 cm^{-1}, 1041 cm^{-1}, 1091 cm^{-1}, 1165 cm^{-1} and 1248 cm^{-1}. All these vibrational modes correspond to intrinsic to PC molecule. In case of *g*-PC, out of plane C-H bending and wagging modes were completely absent (indicated by red arrow) and may be attributed to substrate effect[7,8]. In addition to the C-C stretching mode which indicate the in plane vibration of carbon atoms in graphene lattice, C-O, C=O and C-H etc. vibrations were also observed in *g*-PC. Importantly, considerable shifts in IR peaks ($\Delta\omega$) were observed in case of *g*-PC as compared to that of bare PC such as, in C-C stretching mode ($\Delta\omega$ ~80 cm^{-1}) and C=O vibrational modes ($\Delta\omega$ ~50 cm^{-1}). Broadening in IR peaks can also be observed in case of *g*-PC (see peaks labeled as 4, 6 and 7 etc.). Shift and broadening in IR peaks, in case of *g*-PC as compared to bare PC is a clear indication that graphene is functionalized[6] with PC molecules. We have also observed similar effects of functionalization in other high *k* solvents (acetone and DMF). IR data indicate that graphene layers exfoliated in acetone, DMF and PC are functionalized due to covalent bond formation between solvent molecule and carbon atoms in graphene. These covalent bonds are eventually responsible for doping induced disorders.

Comparison between IR spectra of graphene layers exfoliated in low *k* and high *k* solvents suggest that covalent attachment of solvent molecules with graphene is the preliminary reason behind excess dopants in graphene layers exfoliated in high dielectric solvents. These excess dopants also result in decrease in inter defect distance (L_D) and hence the carrier mobility.

S8.0 References:

1 A K. M. Newaz, Y. S. Puzyrev, B. Wang, S. T. Pantelides and K. I. Bolotin, *Nat. Commun.*, 2012, **3**, 734.

2 C. Casiraghi, *Physica S. Solidi*. 2009, **7**, 175–177.

3 P. Kumar Srivastava and S. Ghosh, *Appl. Phys. Lett.*, 2013, **102**, 043102.

4 A. Hirsch, J. M. Englert, F. Hauke, *Acc. Chem. Res.* 2013, **46**, 87–96.

5 B. Ankamwar, F. Surti, *Chem. Sci. Trans* 2012, **1**, 500–507.

6 C. Galande, A. D. Mohite, A. V Naumov, W. Gao, L. Ci, A. Ajayan, H. Gao, A. Srivastava, R. B. Weisman and P. M. Ajayan, *Sci. Rep.*, 2011, **1**, 85.

7 Hsu, C. S.; Infrared Spectroscopy, Chapter 15. "*Hand Book for Instrumental techniques and Analytical Chemistry*" 247–284.

8 B. C. Postmus, K. Nakamoto, J. R. Ferraro, J. R. Ferrarn, *Inorganic Chemistry* 1967, **6**, 2194.